ORIGINAL PAPER

Carbazole-based donor materials with enhanced photovoltaic parameters for organic solar cells and hole-transport materials for efficient perovskite solar cells

Shehla Gul[1] · Shanza Hameed[1] · Muhammad Ans[1] · Javed Iqbal[1]

Abstract

Five carbazole-based donor molecules are designed by structural engineering of reference molecule PF. The molecules are devised by substitution of thiophene bridged end-capped acceptor groups namely (2-methylenemalononitrile) PF1, (methyl 2-cyanoacrylate) PF2, (3-methyl-5-methylene-2-thioxothiazolidin-4-one) PF3, (2-(3-methyl-5-methylene-4-oxothiazolidin-2-ylidene) malononitrile) PF4, and (4-(5-methylthiophen-2-yl) benzo[c] [1, 2, 5] thiadiazol) PF5. A DFT investigation was performed at the selected DFT functional MPW1PW91/6–31G (d,p) to investigate the optoelectronic properties of PF and all designed (PF1-PF2) molecules. Several important characteristics, i.e., band gap (E_g), transition density matrix analysis, dipole moment (μ), density of states analysis, reorganization energies, open circuit voltage (V_{oc}), and fill factor, were investigated. The comparison of energy levels of reference molecule and designed molecules unveils the fact that these molecules are efficient hole transport materials to be used in perovskite solar cells (PSCs). All the newly drafted molecules (PF1-PF5) show higher λ_{max} values in solvent (Chlorobenzene) ranging from 529 to 614 nm than the reference PF (344 nm). Smaller band gap (E_g) values in a range of 2.27–1.9 eV for newly designed molecules are observed which are very much reduced when compared to reference PF. Lowered exciton binding energies (E_b) and reorganization energies for the electron (0.004279–0.0103337 eV) as compared to PF reveal that our molecules display higher electron mobility rates, and hence, these small molecules can be used as proficient donor materials in high-performance organic solar cells (OSCs) and better hole transport materials (HTMs) for possible application in perovskite solar cells.

Keywords Organic solar cells; Carbazole · Density functional theory

Introduction

Recently used energy sources worldwide include petroleum, crude oil, water, and coal, although these have highly hazardous impacts on all over the world environment. Moreover, because of the over usage, these energy sources are rapidly diminishing with each passing day [1]. Therefore, it is required to shift toward sustainable energy sources that are environmentally friendly. Wind power, biomass, hydro power, and solar are some of the substitute renewable energy sources and are environment friendly as well [2]. Among different renewable energy sources, solar energy is the best appealing because it is ecologically safe, limitless, free of carbon, and can be converted into electrical power using photovoltaic devices [3]. Various technologies are being used based on this principle; among these, the most dominant one is the organic photovoltaics (OPVs) because of their economic aspect, adaptability, and semi-transparency [4–10].

Varieties of solar cells are organic solar cells (OSC), amorphous silicon solar cells, dye-sensitized solar cells, hybrid inorganic–organic solar cells, and perovskite solar cells, etc. [11]. In many solar cells, silicon-based inorganic materials are being used owing to the extreme stability and high power conversion efficiency (PCE) of them, but they have some drawbacks as well such as high cost and having compact structure [10, 12–14]. Recently, OSCs have gained much attention because of their esthetic properties

✉ Muhammad Ans
ansbhatti24@gmail.com

✉ Javed Iqbal
Javedkhattak79@gmail.com; Javed.Iqbal@uaf.edu.pk

1 Department of Chemistry, University of Agriculture, Faisalabad 38000, Pakistan

like easy fabrication process, semi-transparency, flexibility, cost-effectiveness, tunable energy levels along with increased PCE up to 18% [15–17]. Different strategies have been adopted to manufacture high-efficiency OSCs such as by using p–n junction-based material to design the OSCs [18]. These single-layered organic solar cells have been reported for higher (15%) [19] efficiency. Second is by using a donor–acceptor amalgamated layer, and the third strategy is the bulk heterojunction organic solar cells. Mainly, they are made of conjugated polymers and fullerene equivalents and due to their lightweight and less cost, they offer a crucial revelation for tackling the global power crisis [20]. However, because of the reduced band gaps and poor absorption in visible range, the non-fullerene alternatives are leading for the previous few decades [21–24]. Non-fullerene acceptors (NFAs) are currently a prominent focus of research in bulk-heterojunction organic solar cell development. Fullerene is derived from another type of acceptor-molecule that was employed as the primary acceptor material in bulk hetero-junction organic photovoltaic cells. NFA-based OSCs have higher thermal and photochemical stability, as well as longer device lifetimes [25]. Low voltage loss of NFAs and tunable optoelectronic properties along with great synthetic flexibility and full spectral coverage meet the need of power shortage and enable to attain power conversion efficiency (PCE) up to 17% [24, 26–32].

Moreover, the problem with OSCs is the lower efficiency of OSCs than other inorganic material–based solar devices. The reason for this is the very large band gap of organic semi-conductors as compared to the inorganic semiconductors [33]. Due to this reason, metal halide perovskites have now turned out to be the point of enormous interests in photovoltaics [34–37] because of their low cost, high exciton diffusion, strong light absorption properties, and high charge mobility [38–40]. Although perovskite solar cells (PSCs) have exhibited PCE of over 20% [41], the major problem for marketing of perovskite solar cell is the deficient stability caused by commonly employed hole-transport materials (HTMs) alongside dopants as these dopants are costly and allow moisture and ion diffusion which cause the degradation of stability. Consequently, the fabrication of dopant-free HTMs is required. Until recently, many advances have been made in cross-linked, polymer and smaller molecules involved in HTMs. So, this current research aims to select suitable organic materials having usage as HTMs in perovskite solar cells and donating materials for proficient organic solar cell.

In our current study, by the end-capped engineering of PF [34], five small donor molecules namely PF1, PF2, PF3, PF4, and PF5 have been considered. The structural modification has been made by one-sided substitution of methoxy groups of PF with diverse acceptor moieties. All the planned molecules consist of PF

as donating group and thiophene bridged end-capped acceptor groups namely (2-methylenemalononitrile) PF1, (methyl 2-cyanoacrylate) PF2, (3-methyl-5-methylene-2-thioxothiazolidin-4-one) PF3, (2-(3-methyl-5-methyl-ene-4-oxothiazolidin-2- ylidene) malononitrile) PF4, and (4-(5-methylthiophen-2-yl) benzo[c] [1, 2, 5] thiadiazol) PF5. Our current study describes concepts for planning largely effective small molecules as donating materials for competent organic solar cells and HTMs for perovskite solar cells (PSCs).

Computational details

All the calculations are done using Gaussian 09 program, and Gauss view program is used to visualize the results [42]. Density functional theory (DFT) was used for structural optimization of reference and performed using B3LYP [43], CAM B3LYP [44], MPW1PW91, and ωB97XD [45] levels of theory and 631G (d,p) basis set. For investigating the absorption profile of reference molecules, TD-DFT calculations were achieved at same B3LYP, CAM B3LYP, MPW1PW91, ωB97XD levels and 6–31G (d,p) basis set. The absorption maximum of reference molecule is then compared to the experimental value and among four methods, MPW1PW91/6–31G (d,p) level of theory has manifested the nearest value with the experimental value. Hence, the absorption profile of all architecture molecules has been investigated in both the gaseous and solvent (chlorobenzene) medium employing MPW1PW91/6–31G (d,p) level of theory.

The frontier molecular orbital analysis, TDM and DOS analysis, dipole moment (μ), reorganization energies (RE), and charge transfer study of the model and all freshly prepared compounds are performed at MPW1PW91/6-31G (d,p) functional. The TDM and DOS are obtained using Multiwfn 3.7 software and PyMolyze 1.1 software packages, correspondingly [46, 47]. Optimized cationic and anionic structures were obtained by employing MPW1PW91/6-31G (d,p) for the calculation of reorganization energy (RE), for electron (λ_e), and hole (λ_h) using Eqs. (1) (2) [48].

$$\lambda e = \left[E_0^- - E_- \right] + \left[E_-^0 - E_0 \right] \tag{1}$$

$$\lambda h = \left[E_0^+ - E_+ \right] + \left[E_+^0 - E_0 \right] \tag{2}$$

E_0 is the single point energy of neutral molecule optimized at ground level. E_0^-, E_0^+ are ground-state energies of anions and cations obtained from neutral molecule, and E_+^0, E_-^0 represent energy values of cation and anion calculated from cationic and anionic optimized structures.

Results and discussions

Initially, the reference molecule is optimized at four different DFT methods B3LYP, CAM B3LYP, MPW1PW91, ωB97XD levels and 6–31G (d,p) basis set. The value of absorption maximum for reference molecule PF is calculated at four distinctive levels of theory. The experimental value of $\lambda_{\max}$ (336 nm) is found in agreement with the MPW1PW91/6-31G (d,p) functional. Hence, all the calculations herein are performed by employing MPW1PW91 DFT method and 6-31G (d,p) basis set. The chemical structures of all currently investigated molecules are shown in Scheme 1.

Frontier molecular orbital analysis

The optimized geometries of all the designed molecules along with reference molecule have been shown in Figure S1 (Supporting Information).

FMO (frontier molecular orbital) analysis is a technique that estimates the electron charge density distribution around the highest molecular orbital (HOMO) and lowest unoccupied molecular orbital (LUMO). Moreover, the electronic properties of a system are investigated by performing FMO analysis. The FMOs of planned molecules and the reference PF molecule have been presented in Fig. 1. From Fig. 1, it is observed that the HOMO and LUMO of the reference molecule are scattered on half portion of the donor part while in our designed molecules, the HOMO is spread on half of the donor section and LUMO lies on the entire acceptor fragment as shown. The substitution of acceptor end groups has influenced the charge density distribution, and hence, charge transfer occurs from the donor fragment to acceptor end moieties. The charge density is distributed on the acceptor segment in all planned molecules. The HOMO energy values for all designed molecules are discovered as PF (-4.71 eV) > PF5 (-4.78 eV) > PF2 (-4.83 eV) > PF3 (-4.86 eV) > PF4 (-4.87 eV) > PF1 (-4.94 eV), and the LUMO values reported are PF (-0.66 eV) > PF5 (-2.51 eV) > PF2 (-2.61 eV) > PF3 (-2.67 eV) > PF4 (-2.97 eV) > PF1 (-2.99 eV). The HOMO $-$ LUMO band gap energies explored are PF (4.05 eV) > PF5 (2.27 eV) > PF3 (2.24 eV) > PF2 (2.22 eV) > PF1 (1.95 eV) > PF4 (1.9 eV). Among all the planned molecules, PF4 has reported the lowest band gap owing to the presence of Cyano (CN) containing (2-methylene malononitrile) acceptor unit that is responsible for the auspicious charge transmission from HOMO to LUMO.

From these interpretations, we can conclude that all our designed molecules possess excellent charge transfer properties due to the strong electron-pulling substituents.

To achieve the PSCs with enhanced performance, comparison of energy levels of perovskite and HTMs is a crucial factor [49]. The HOMO–LUMO energy level diagram of planned molecules and perovskite has been shown in Fig. 2. The determined HOMO levels for PF, PF1-PF5 HTMs are -4.71, -4.94, -4.83, -4.86, -4.87, and -4.78 eV, correspondingly. These values are considerably larger than the HOMO of perovskite (-5.43 eV) that suggest higher hole-extraction [49], and the LUMO values for PF, PF1-PF5 HTMs (-0.66, -2.99, -2.61, -2.62, -2.97, and -2.51 eV) are sufficiently higher than the LUMO value of perovskite (-3.92 eV). Consequently, the transfer of undesired electrons from perovskite to counter electrode will be suppressed, and therefore, the charge recombination reduces [50]. These results demonstrate that these PF-based molecules are efficient for using as HTMs for high-performance PSCs.

TDM and exciton binding energy (E_b)

The utmost influential technique for evaluation of electronic excitation processes including diffusion, creation, recombination, and separation of charges is transition density matrix (TDM) analysis [51]. TDM analysis aims to validate the quantum geometry of compounds when excitation occurs. This analysis reveals the relationship between donor and acceptor groups in excited state [52]. TDM represents the density of electronic distribution in a molecule along with the transitory location of holes and electrons in the compound during excitation [53]. TDM analysis of the PF molecule and newly designed compounds (PF1-PF5) has been computed at 6-31G (d,p) using selected functional hybrid of DFT and is presented in Fig. 3 as two-dimensional colored plot using Multiwfn 3.6 software package. The reference molecule was sectioned apart as donor and acceptor regions labeled by D and A respectively. The designed molecules have been divided into four parts as donor, acceptor-1, acceptor-2, and spacer regions designated by D, A1, A2, and S respectively as shown in Fig. 3. As presented in TDM graphs, the standard straight x-axis and left upright y-axis exhibit the numbering of all the atoms present in the molecule excluding hydrogen atoms, as hydrogen atoms have been ignored by default during numbering of atoms because of their insignificant influence in the electronic excitations. On the other hand, the right y-axis is presenting the increasing electronic charge density from blue to red color in upper course. In the reference (PF) molecule, charge consistency is constantly confined in the donor region. While in the designed molecules (PF1-PF4), more charge consistency is seen in acceptor and spacer regions.

Another parameter exciton (electron–hole pair) binding energy that determines the photophysical and
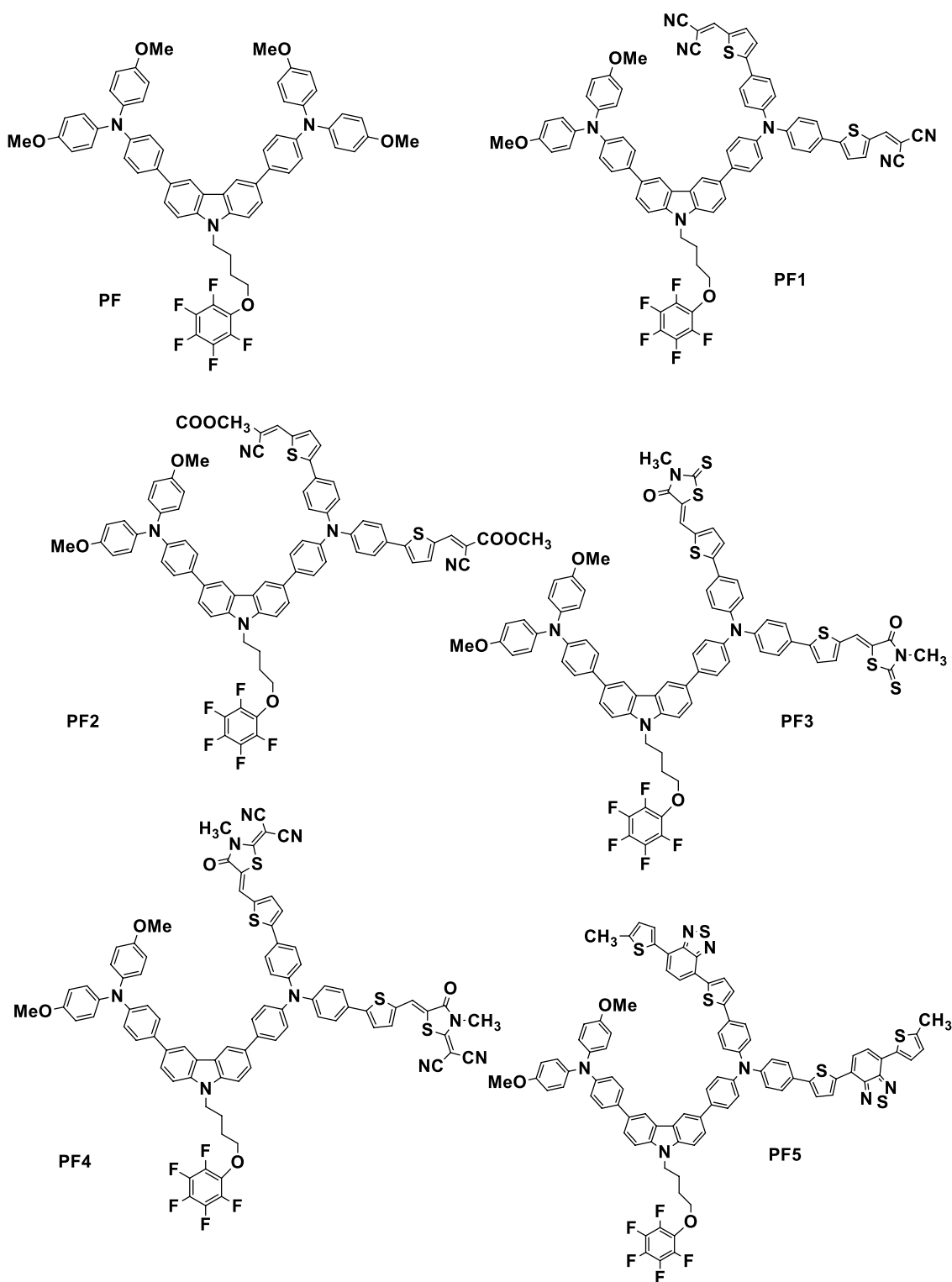
Scheme 1 Chemical structures of PF and architecture molecules (PF1-PF5)

opto-electronic properties of devised compounds is defined as the amount of energy to estimate the exciton dissociation potential [54]. Binding energy and columbic interaction are in direct relation with each other. The lesser will be the binding energy, the lower is the columbic interaction that results in higher power conversion efficiency by escalating
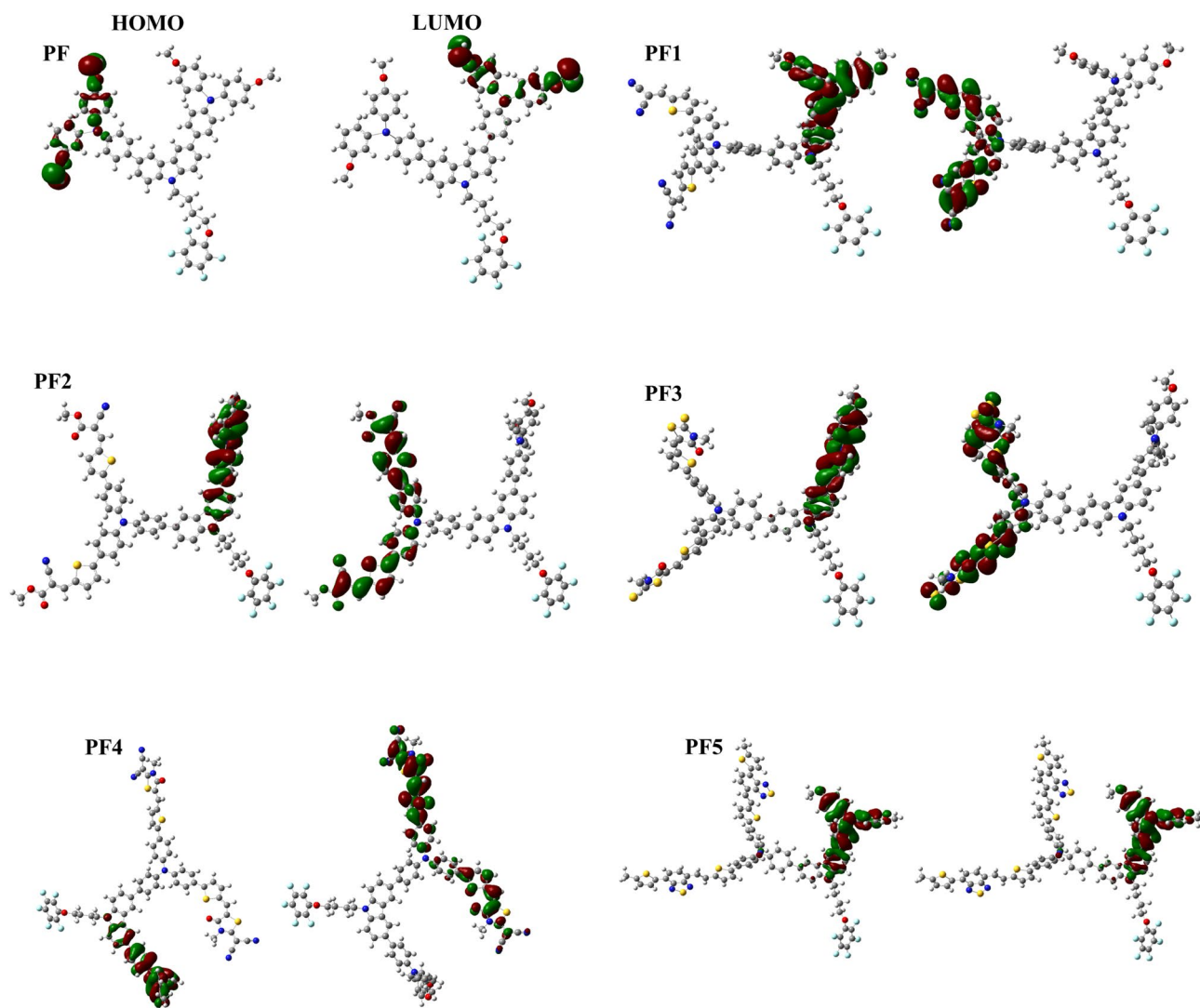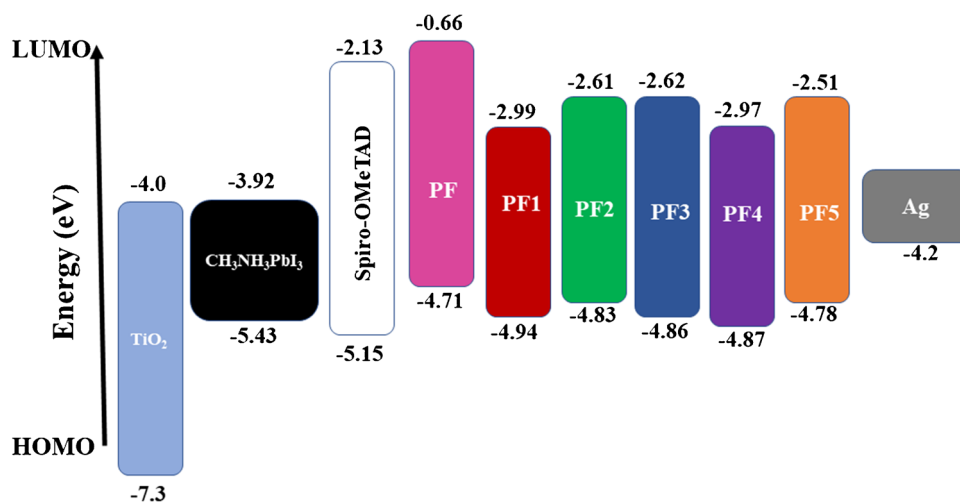
Fig. 1 FMOs of reference and all architecture molecules

Fig. 2 Energy level diagram of PF-PF5 HTMs and perovskite
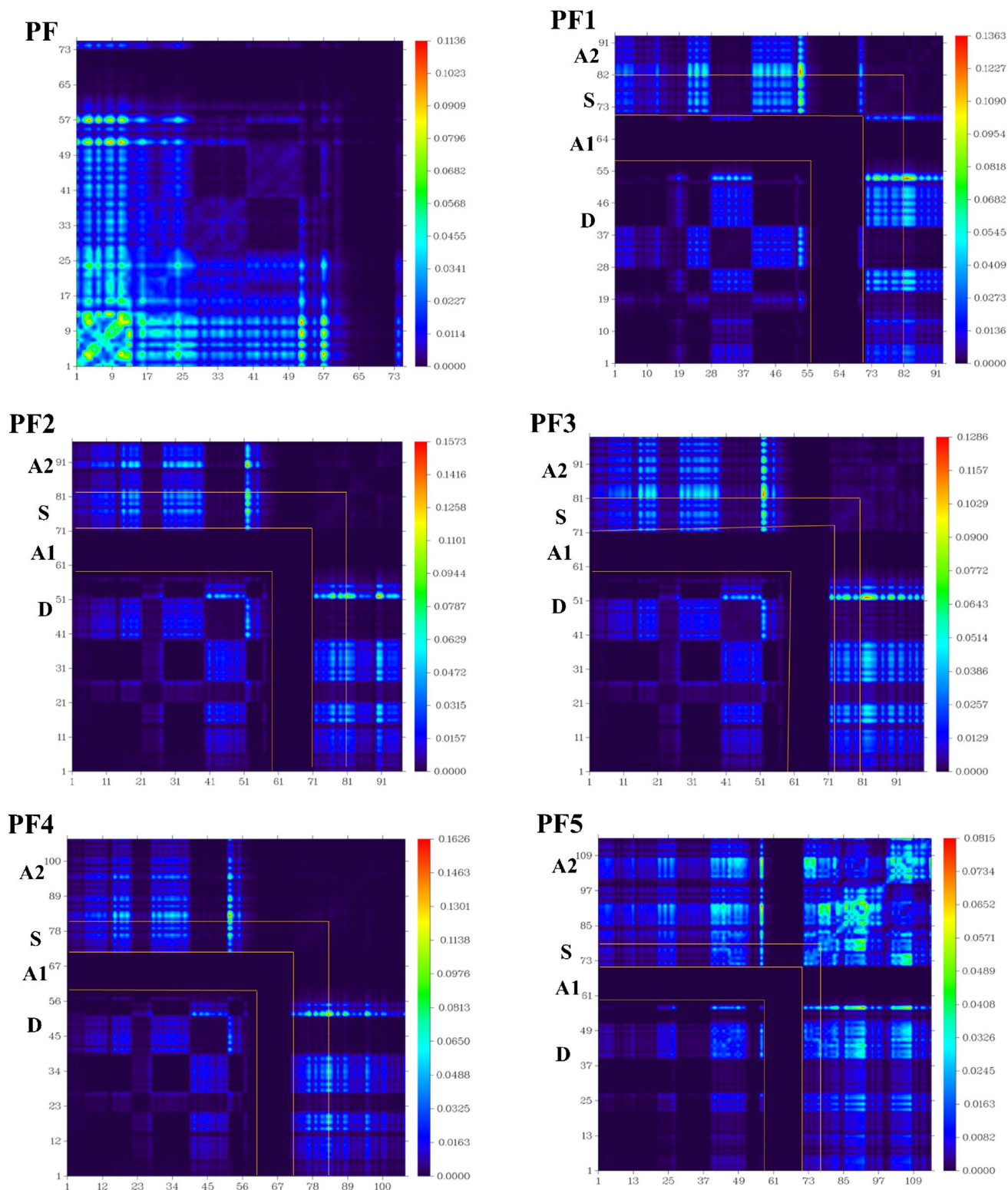
Fig. 3 TDM plots for reference PF and designed molecules

Table 1 Contribution of acceptor and donor in raising the HOMO and LUMO of model PF and designed (PF1-PF5) molecules

Molecules	HOMO=H LUMO=L	Acceptor (eV)	Donor(eV)	Spacer (eV)
PF	H	0.0	100	–
	L	3.4	96.6	–
PF1	H	48.1	14.5	37.4
	L	0.0	100.0	0.0
PF2	H	46.7	15.8	37.5
	L	0.0	100.0	0.0
PF3	H	61.2	11.1	27.7
	L	0.0	99.9	0.0
PF4	H	61.4	10.2	28.4
	L	0.0	100.0	0.0
PF5	H	89.3	2.7	8.0
	L	1.0	98.0	1.0

the charge dissociation rate. The binding energies calculated using Eq. 3 [55] for all designed molecules in gaseous and solvent both (chlorobenzene) media have been reported in Tables 1, 2 and 3.

$$E_b = E_g - E_x \tag{3}$$

In Eq. 3, E_g symbolizes the band gap energy, and E_x is the transition energy of first excited state.

DOS analysis

The density of states (DOS) investigation provides a map for charge transfer and determines the electronic charge distribution on HOMO and LUMO. The plotted DOS

diagrams for reference and all architecture compounds are displayed in Fig. 4. It comprises a horizontal axis expressing energy in eV (electron volts) and a perpendicular axis for relative intensity. The negative values on plane x-axis represent conduction band HOMO, and the valence band LUMO is expressed by right positive values on the x-axis of the DOS plots, and the region indicated by dotted lines indicates the band gap energy (E_g) value of molecules. It explains the contribution of different fragments, i.e., acceptor, donor, and spacer represented by A1, A2, D, and S in raising the HOMO and LUMO of a molecule in the excited state. The DOS analysis was performed for all molecules by using the selected DFT functional and basis set. The contribution of all fragments in raising the HOMO and LUMO of all molecules is summarized in Table 1.

It can be seen from the tabulated data that in raising the HOMO of all the investigated molecules, the major contributor is acceptor and spacer along with a minor role of donor fragment, while in the formation of LUMO, donor fragment is contributing majorly with a small participation of acceptor and spacer fragments as illustrated in Table 1.

Dipole moment (μ)

Dipole moment determines the polarity and dissolution of molecule in organic solvent [56–59]. The dipole moment expresses the polarity of molecules, it has a direct relation with the dissolution rate, and the greater the dipole moment, the greater will be the dissolution of molecule

Table 2 Calculated λ_{max}, transition energy (ΔE) oscillator strength (f_0) and C.I. (%) in gaseous medium

Molecules	Calculated λ_{max} (nm)	Experimental λ_{max} (nm)	ΔE (eV)	f_0	Transitions	C.I (%)	E_b (eV)
PF	339	337	3.7864	0.6334	L→L+4	58%	0.55
PF1	511	–	2.2887	0.8200	H-1→L	69%	0.25
PF2	491	–	2.4109	0.9630	H-1→L	69%	0.32
PF3	522	–	3.1023	0.5345	H-3→L+1	66%	0.24
PF4	545	–	3.0212	0.6357	H-4→L	50%	0.3
PF5	592	–	2.0715	0.3827	H-1→L+1	54%	0.37

Table 3 Calculated λ_{max}, transition energy (ΔE) oscillator strength (f_0), and C.I (%) in solvent (chlorobenzene) medium

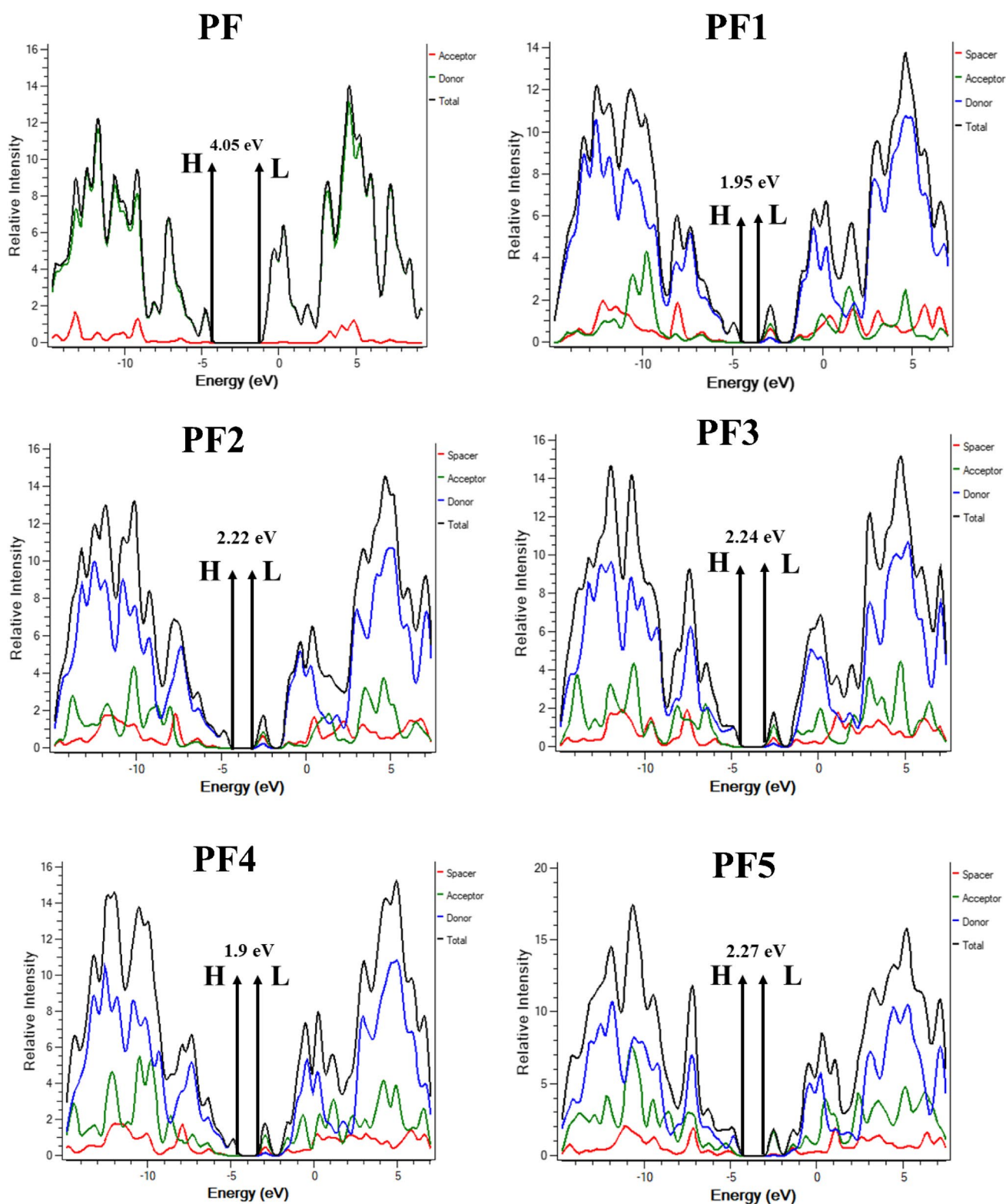| Molecules	Calculated λ_{max} (nm)	Experimental λ_{max} (nm)	ΔE (eV)	f_0	Transition	C.I (%)	E_b (eV)
PF	344	336	3.5262	1.2542	L+1→L+3	61%	0.65
PF1	556	–	2.1243	0.9931	H-1→L	68%	0.15
PF2	529	–	2.4670	0.5216	H-1→L+1	69%	0.32
PF3	558	–	2.3257	0.3486	H-3→L+1	63%	0.14
PF4	581	–	2.0826	1.5806	H-1→L	66%	0.1
PF5	614	–	2.0185	0.5840	H-1→L+1	56%	0.33

Fig. 4 DOS plots for PF and all designed molecules

in polar solvent [60]. All the architecture molecules have reported the highest degree of dipole moment than the reference molecule in excited state. This upsurge in

dipole moment proves the factor that all molecules are placed in a manner to lower the charge recombination and escalate the fill factor. The reported dipole moment
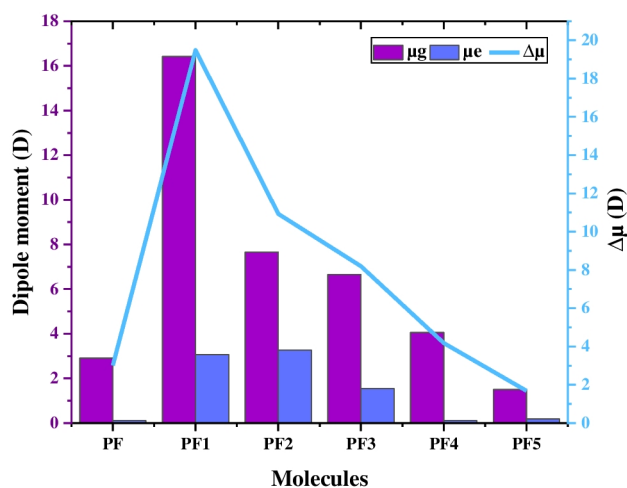
Fig. 5 Graphical presentation of dipole moment (μ) in ground state, excited state, and difference between them
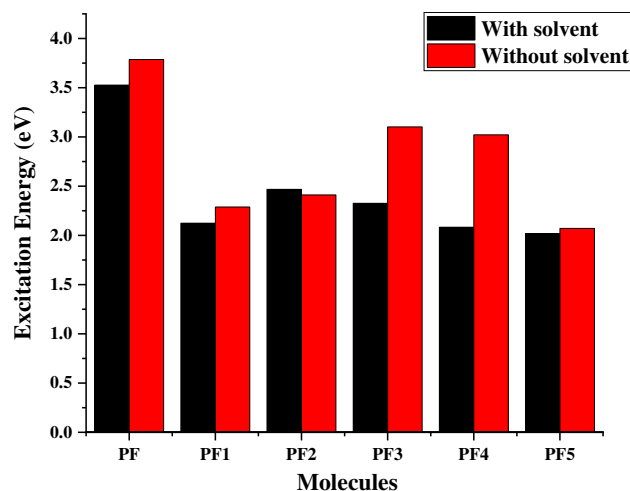
Fig. 7 Pictorial view of excitation energy in ground and excited state
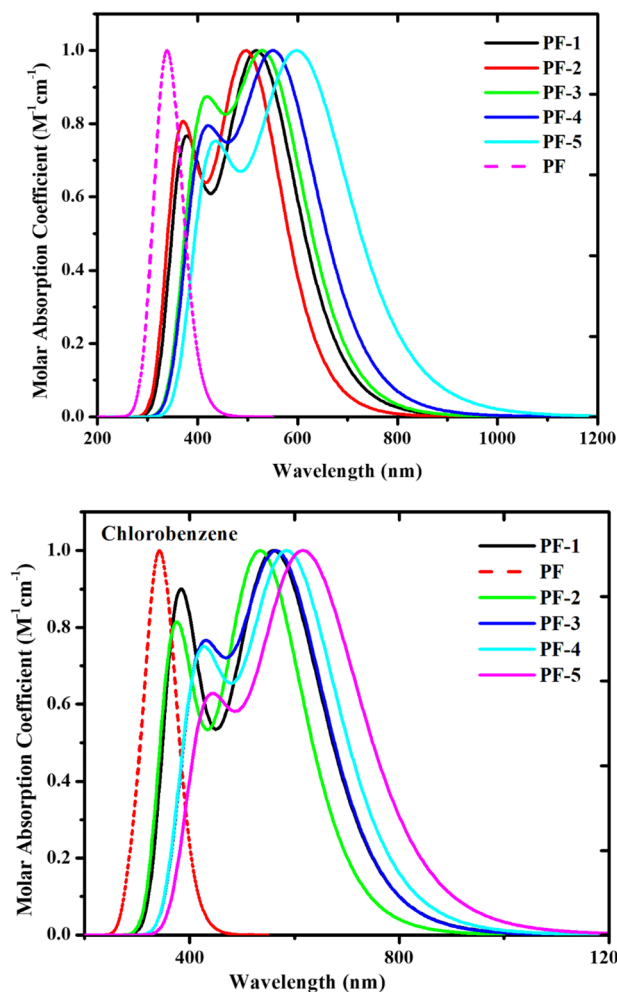
Fig. 6 UV–Visible spectra of investigated molecules in gaseous and solvent (chlorobenzene) medium

in chlorobenzene for all architecture molecules ranges in 1.6845–19.4845 D. Among all the reported molecules, PF1 has explored the maximum dipole moment owing to its greater solubility in chlorobenzene and the polar regions' presence in the structure, reducing the charge recombination and making multilayer fabrication easy. The dipole moment of devised molecules in gaseous state lies in the range 1.5046–16.4192 D. The graphical view of dipole moment has been shown in Fig. 5.

Absorption analysis

Absorption of light and harvesting are two core parameters that have gained interests of researchers in production of solar energy. The UV–Visible spectra must be evaluated because they provide an understanding about the charge transfer analysis and electronic excitations [54, 61, 62]. The evaluated absorption spectra of all architecture molecules in gaseous and solvent medium are displayed in Fig. 6 and their excited state energies are shown in Fig. 7. In the current research, the absorption spectra of all designed molecules have been simulated via TD-DFT calculations in IEFPCM model, and the outcomes are tabulated in Tables 2 and 3 respectively.

The absorption analysis demonstrates that all the architecture molecules have reported a greater value of λ_{max} in comparison to the model molecule PF. The absorption maxima have an inverse relation with the band gap value. A lesser band gap value causes the higher λ_{max} value and vice versa. And hence, all the investigated molecules have reported higher λ_{max} values. C.I. is the percentage of excitation from HOMO to LUMO. The molecules with lower C.I have less charge dissociation rate and vice versa. Among all our designed molecules, PF1, PF2, PF3, and PF4 have

higher percentage of interactions between highest occupied molecular orbital and lowest unoccupied molecular orbital compared to reference molecule, which cause the dissociation of photons easier, and the PCE can be improved.

These results reveal that all the freshly planned molecules are accompanied by strong electron-extracting species. The absorption values for all molecules in gaseous state follows PF (339 nm) < PF2 (491 nm) < PF1 (511 nm) < PF3 (522 nm) < PF4 (545 nm) < PF5 (592 nm). And for the solvent medium, it follows PF (344 nm) < PF2 (529 nm) < PF1 (556 nm) < PF3 (558 nm) < PF4 (581 nm) < PF5 (614 nm).

MEP surfaces

Molecular electrostatic potential surface conveys a good concept about the charge transfer from donor to acceptor moieties. The molecular electrostatic potential (MEPs) of all the analyzed compounds demonstrate that the blue color is spread largely over the central part whereas the red color is existing on the end-capped acceptor areas. The oxygen atoms in molecules present on the terminals are highlighted with red color indicating the region of concentrated electronic charge. Similarly, the cyano (CN) groups are blue colored owing to the nitrogen atoms present on the terminals of the molecules that indicates the nucleophilic reaction site with strong electron cloud. The MEPs of the reference (PF) along with all newly designed molecules have been computed at the selected DFT functional MPW1PW91/6-31G (d,p) and are mapped with red and blue hues showing negative and strong positive-charge regions, respectively, as displayed in Fig. 8.

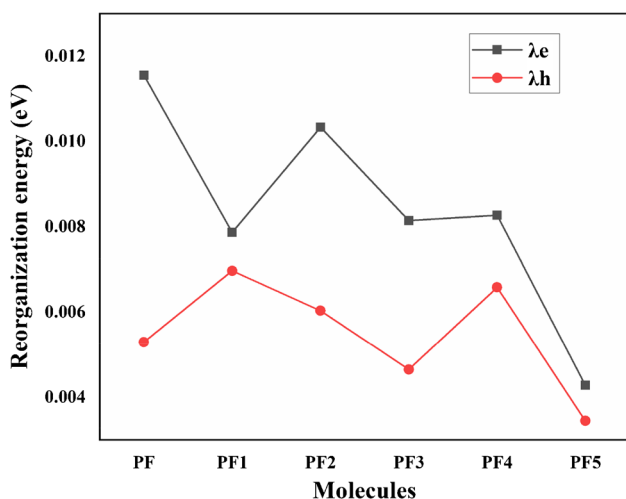**Fig. 8** Colored maps of MEP for PF and designed molecules (PF1-PF5)
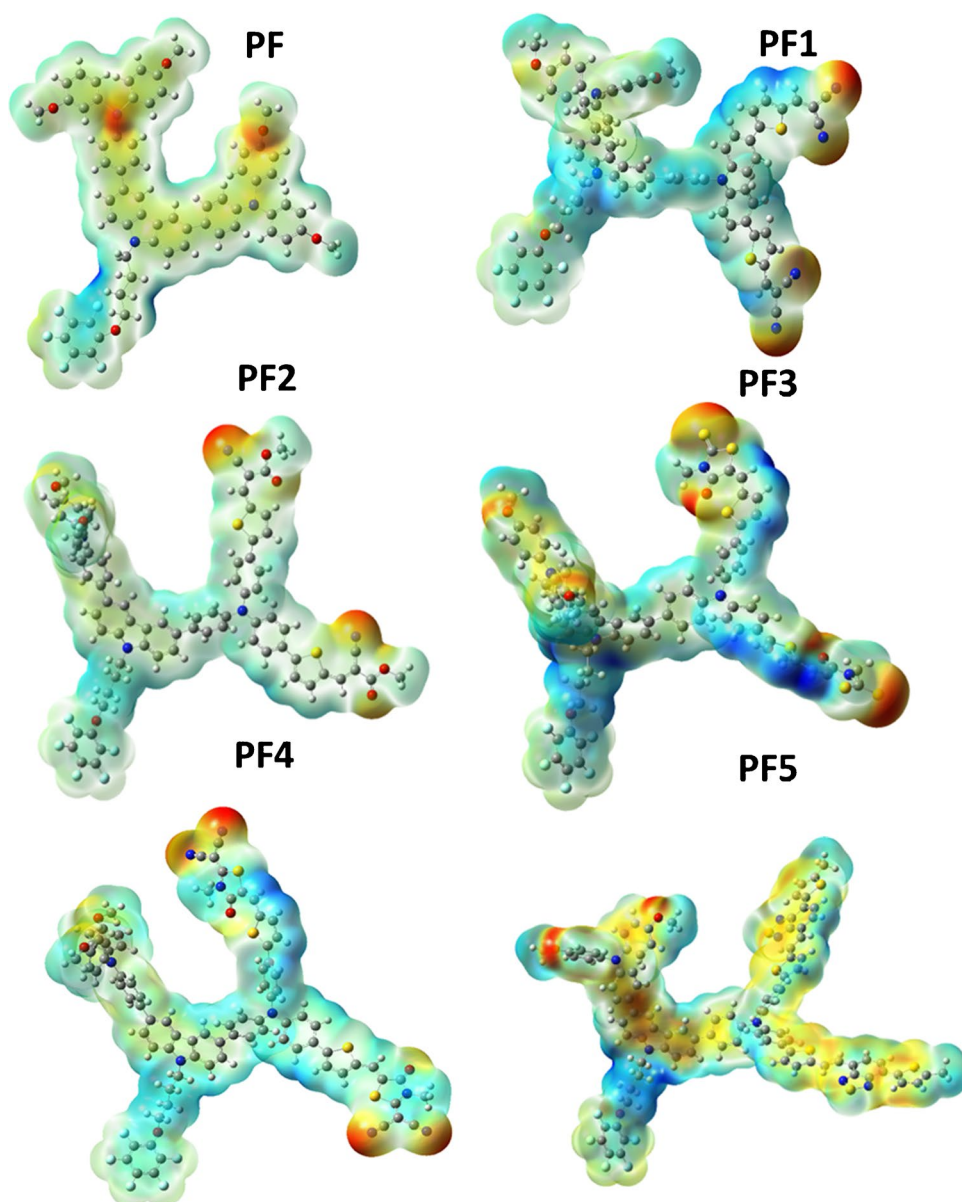
Fig. 9 Graphical representation of reorganization energy (RE)

Table 4 Anion and cation mobilities for PF and all freshly planned molecules

Molecules	λ_e (eV)	λ_h (eV)
PF	0.0115535	0.0052976
PF1	0.0078686	0.0069716
PF2	0.0103337	0.0060354
PF3	0.0081454	0.0046518
PF4	0.0082689	0.0065838
PF5	0.004279	0.0034439

RE

Reorganization energy (RE) is a significant factor which determines the charge transfer properties of a molecule by computing the charge transfer mobilities [48]. The RE plays a vital role in estimating the PCE of OSCs [63]. Reorganization energies are of two types, internal and external reorganization energy. We are only concerned with the internal

reorganization energy due to the insignificant effect of external RE. The graphical representation of reorganization energies is shown in Fig. 9.

The λ_e value for model molecule is 0.0115535 eV. The lower the value of λ_e value, the larger will be the charge transfer rate. Among all the investigated molecules, the lowermost value of λ_e has been showed by PF5. All other designed molecules (PF1-PF4) have also reported the lowest λ_e values than the model PF molecule owing to the strong electron-withdrawing groups. These results support the fact that end-capped acceptor modifications have a strong effect on the interior RE of a molecule. Furthermore, among all architecture molecules, the PF5 has the lowest value of hole reorganization energy (λ_h) which again expresses the high rate of charge transfer. The computed results of electron and hole reorganization energies have been displayed in Table 4.

V_{oc}

Open circuit voltage is a factor that estimates the current of solar devices [64]. It is defined as the maximum amount of current that is taken out from a device. To find the best use of our investigated molecules as donor in organic solar cells, we have chosen $PC_{16}BM$ acceptor for calculation of V_{oc}. The HOMO value for $PC_{16}BM$ acceptor is -6.1 eV and its LUMO value is -3.7 eV. V_{oc} is evaluated using Eq. 4 [65] and is graphically shown in Fig. 10. The V_{oc} values computed for all the designed molecules have been presented in Table 5.

$$V_{oc} = \frac{\text{ELUMO of acceptor} - \text{EHOMO of donor} - 0.3}{e}$$

(4)

FF and PCE

Fill factor (FF) is another parameter that determines the PCE of OSCs. The fill factor for designed molecules has been calculated using Eq. (5) [66]:

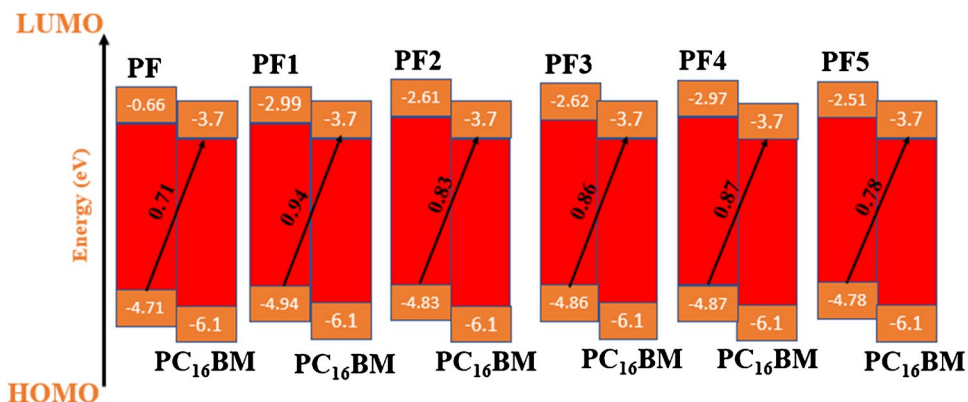**Fig. 10** Graphical representation of open circuit voltage (V_{oc})

Table 5 Calculated open circuit voltage V_{oc}, normalized V_{oc}, fill factor (FF), percentage FF (FF%), and PCE for reference and architecture molecules

Molecules	V_{oc} (eV)	Normalized V_{oc} (eV)	FF	FF%	PCE
PF	0.71	2.765	0.40	40%	6.10
PF1	0.94	3.661	0.46	46%	9.29
PF2	0.83	3.233	0.43	43%	7.67
PF3	0.86	3.351	0.44	44%	8.13
PF4	0.87	3.389	0.45	45%	8.41
PF5	0.78	3.038	0.42	42%	7.04

$$FF = \frac{\frac{eV_{oc}}{K_B T} - \ln(\frac{eV_{oc}}{K_B T} + 0.72)}{\frac{eV_{oc}}{K_B T} + 1} \quad (5)$$

The equation of FF has $\frac{eV_{oc}}{K_B T} = V_{oc}$, a normalized open-circuit voltage in which e is the elementary charge fixed at 1 in the current study. V_{oc} is voltage estimated by Eq. (4), K_B is Boltzmann constant whose value is $8.61733034 \times 10^{-5}$ electron volts/kelvin, and T is temperature whose value was fixed at 300 K [67, 68]. The computed FF results for all studied molecules are summarized in Table 5.

Power conversion efficiency investigation is a strategy that ensures the efficacy of solar cell materials for practical applications. The PCE computed for all molecules using Eq. (6), and the results are displayed in Table 5:

$$PCE = \frac{J_{sc} V_{oc} FF}{P_{in}} \quad (6)$$

In the above equation, J_{sc} is the short circuit current and its value (21.5 mA/cm^2) has been taken from reference paper [34]. This value has been assumed for all the designed molecules. The factor P_{in} is the power of the incoming rays whose value is fixed at 100 mW cm^{-2}. Among all the investigated molecules, PF1 molecule has better PCE than all other designed molecules due to the significantly higher values of V_{oc}, FF, and normalized V_{oc} that relates directly with PCE.

Conclusion

In the current research, we aim for carbazole-based small molecules as donor materials for use in OSCs and as HTMs for efficient perovskite solar cells. All the calculations were performed at selected MPW1PW91/6–31G (d,p) DFT functional. The designed molecules (PF1-PF5) have reported impressive results. PF1-PF5 have explored lower band gap values (2.27–1.9 eV), alongside higher λ_{max} values of (529–614 nm) in chlorobenzene solvent. All the reported

molecules have manifested higher values of dipole moment ranging from 4.7190 to 19.4845 D in chlorobenzene showing their better solubility in organic solvent and least charge recombination. The smaller values of RE reported for all the designed molecules indicate high charge mobility rate of these molecules. The V_{oc} calculated for all designed molecules when scaled with PC$_{16}$BM acceptor are higher than the reference molecule. This suggests that all the newly designed molecules can achieve better performing efficiency. All the studied molecules have higher anticipated PCE values by scaling up with PCBM (7.04–9.29%) than the reference molecule PF (6.10%) suggesting that these molecules can be proved effective donor materials for future organic solar cells, and the HOMO LUMO energy level and reorganization energy values show that these designed PF-based molecules can be effective HTMs for use in upcoming elite PSCs.

Declarations

References

1. Irfan M et al (2017) Design of donor–acceptor–donor (D–A–D) type small molecule donor materials with efficient photovoltaic parameters. Int J Quantum Chem 117(10):e25363

2. Green M (2001) Clean electricity from photovoltaics Vol. MD Archer and R. Hill., Singapore: World Scientific

3. Vogiatzoglou N (2007) The importance of embodied and operational energy and the use of renewable energy systems (RES) in

the domestic sector in Greece: case study, analysis of a design for a private residence in Athens. University of London, University College London (United Kingdom)

4. Mahmood A (2019) Photovoltaic and charge transport behavior of diketopyrrolopyrrole based compounds with A–D–A–D–A skeleton. J Cluster Sci 30(4):1123–1130

5. Mahmood A et al (2019) First-principles theoretical designing of planar non-fullerene small molecular acceptors for organic solar cells: manipulation of noncovalent interactions. Phys Chem Chem Phys 21(4):2128–2139

6. Mahmood A, Khan SU-D, Rana UA (2014) Theoretical designing of novel heterocyclic azo dyes for dye sensitized solar cells. J Comput Electron 13(4):1033–1041

7. Mahmood A et al (2018) Introducing four 1, 1-dicyanomethylene-3-indanone end-capped groups as an alternative strategy for the design of small-molecular nonfullerene acceptors. J Phys Chem C 122(51):29122–29128

8. Mahmood A, Abdullah MI, Khan SU-D (2015) Enhancement of nonlinear optical (NLO) properties of indigo through modification of auxiliary donor, donor and acceptor. Spectrochim Acta Part A Mol Biomol Spectrosc 139:425–430

9. Mahmood A et al (2019) Red shifting of absorption maxima of phenothiazine based dyes by incorporating electron-deficient thiadiazole derivatives as π-spacer. Arab J Chem 12(7):1447–1453

10. Mahmood A, Irfan A (2020) Effect of fluorination on exciton binding energy and electronic coupling in small molecule acceptors for organic solar cells. Comput Theor Chem 1179:112797

11. Shehzad RA et al (2020) Designing of benzothiazole based non-fullerene acceptor (NFA) molecules for highly efficient organic solar cells. Comput Theor Chem 1181:112833

12. Gong J, Liang J, Sumathy K (2012) Review on dye-sensitized solar cells (DSSCs): fundamental concepts and novel materials. Renew Sustain Energy Rev 16(8):5848–5860

13. Mahmood A et al (2015) Computational designing of triphenylamine dyes with broad and red-shifted absorption spectra for dye-sensitized solar cells using multi-thiophene rings in π-spacer. Bull Korean Chem Soc 36(11):2615–2620

14. Mahmood A, Khan SU-D, urRehman F (2015) Assessing the quantum mechanical level of theory for prediction of UV/Visible absorption spectra of some aminoazobenzene dyes. J Saudi Chem Soc 19(4):436–441

15. Luo Z et al (2020) Fine-tuning energy levels via asymmetric end groups enables polymer solar cells with efficiencies over 17%. Joule 4(6):1236–1247

16. Shehzad RA et al (2021) Enhanced linear and nonlinear optical response of superhalogen (Al7) doped graphitic carbon nitride (g-C3N4). Optik 226:165923

17. Khan AU et al (2021) DFT study of superhalogen (AlF4) doped boron nitride for tuning their nonlinear optical properties. Optik 231:166464

18. Afzaal M, O'Brien P (2006) Recent developments in II–VI and III–VI semiconductors and their applications in solar cells. J Mater Chem 16(17):1597–1602

19. Yuan J et al (2019) Single-junction organic solar cell with over 15% efficiency using fused-ring acceptor with electron-deficient core. Joule 3(4):1140–1151

20. Sun D et al (2015) Non-fullerene-acceptor-based bulk-heterojunction organic solar cells with efficiency over 7%. J Am Chem Soc 137(34):11156–11162

21. He Y, Li Y (2011) Fullerene derivative acceptors for high performance polymer solar cells. Phys Chem Chem Phys 13(6):1970–1983

22. Anctil A et al (2011) Material and energy intensity of fullerene production. Environ Sci Technol 45(6):2353–2359

23. Liu T et al (2016) Ternary organic solar cells based on two compatible nonfullerene acceptors with power conversion efficiency> 10%. Adv Mater 28(45):10008–10015

24. Zhang J et al (2018) Material insights and challenges for non-fullerene organic solar cells based on small molecular acceptors. Nat Energy 3(9):720–731

25. Yan C et al (2018) Non-fullerene acceptors for organic solar cells. Nat Rev Mater 3(3):1–19

26. Wang X et al (2020) Towards multi-center glaucoma OCT image screening with semi-supervised joint structure and function multi-task learning. Med Image Anal 63:101695

27. Liu T et al (2020) Concurrent improvement in J sc and V oc in high-efficiency ternary organic solar cells enabled by a red-absorbing small-molecule acceptor with a high LUMO level. Energy Environ Sci 13(7):2115–2123

28. Zhan L et al (2020) Over 17% efficiency ternary organic solar cells enabled by two non-fullerene acceptors working in an alloy-like model. Energy Environ Sci 13(2):635–645

29. Ma R et al (2020) Adding a third component with reduced miscibility and higher LUMO level enables efficient ternary organic solar cells. ACS Energy Lett 5(8):2711–2720

30. Yao J et al (2020) Cathode engineering with perylene-diimide interlayer enabling over 17% efficiency single-junction organic solar cells. Nat Commun 11(1):1–10

31. Cui Y et al (2020) Single-junction organic photovoltaic cells with approaching 18% efficiency. Adv Mater 32(19):1908205

32. Yu H et al (2020) Tailoring non-fullerene acceptors using selenium-incorporated heterocycles for organic solar cells with over 16% efficiency. J Mater Chem A 8(45):23756–23765

33. Chidichimo G, Filippelli L (2010) Organic solar cells: problems and perspectives. Int J Photoenergy 2010.

34. Canil L et al (2021) Halogen-bonded hole-transport material suppresses charge recombination and enhances stability of perovskite solar cells. Adv Energy Mater 11(35):2101553

35. Zhang X et al (2021) CN-based carbazole-arylamine hole transporting materials for perovskite solar cells: Substitution position matters. J Energy Chem 62:563–571

36. Zhang X et al (2021) Hole transporting material with passivating group (CN) for perovskite solar cells with improved stability. Dyes Pigm 187:109129

37. Liu X et al (2019) Molecular engineering of simple carbazole-triphenylamine hole transporting materials by replacing benzene with pyridine unit for perovskite solar cells. Solar Rrl 3(5):1800337

38. Kojima A et al (2009) Organometal halide perovskites as visible-light sensitizers for photovoltaic cells. J Am Chem Soc 131(17):6050–6051

39. Stranks SD et al (2013) Electron-hole diffusion lengths exceeding 1 micrometer in an organometal trihalide perovskite absorber. Science 342(6156):341–344

40. Xing G et al (2013) Long-range balanced electron-and hole-transport lengths in organic-inorganic CH3NH3PbI3. Science 342(6156):344–347

41. Zhang H et al (2022) High-efficiency (> 20%) planar carbon-based perovskite solar cells through device configuration engineering. J Colloid Interface Sci 608:3151–3158

42. Dennington R, Keith T, Millam J (2008) GaussView 5.0, Gaussian. Inc., Wallingford.

43. Antony J, Grimme S (2006) Density functional theory including dispersion corrections for intermolecular interactions in a large benchmark set of biologically relevant molecules. Phys Chem Chem Phys 8(45):5287–5293

44. Yanai T, Tew DP, Handy NC (2004) A new hybrid exchange–correlation functional using the Coulomb-attenuating method (CAM-B3LYP). Chem Phys Lett 393(1–3):51–57

45. Chai J-D, Head-Gordon M (2008) Long-range corrected hybrid density functionals with damped atom–atom dispersion corrections. Phys Chem Chem Phys 10(44):6615–6620

46. Tenderholt A (2006) PyMOlyze, version 1.1, in Stanford University, CA Stanford

47. Lu T, Chen F (2012) Multiwfn: a multifunctional wavefunction analyzer. J Comput Chem 33(5):580–592

48. Ans M et al (2020) Tuning opto-electronic properties of alkoxy-induced based electron acceptors in infrared region for high performance organic solar cells. J Mol Liq 298:111963

49. Lin Y-D et al (2021) Molecularly engineered cyclopenta [2, 1-b; 3, 4-b′] dithiophene-based hole- transporting materials for high-performance perovskite solar cells with efficiency over 19%. ACS Appl Energy Mater 4(5):4719–4728

50. Lee K-M et al (2022) High-performance perovskite solar cells based on dopant-free hole-transporting material fabricated by a thermal-assisted blade-coating method with efficiency exceeding 21%. Chem Eng J 427:131609

51. Wang D et al (2014) Rational design and characterization of high-efficiency planar A–π–D–π–A type electron donors in small molecule organic solar cells: a quantum chemical approach. Mater Chem Phys 145(3):387–396

52. Farhat A et al (2020) Tuning the optoelectronic properties of subphthalocyanine (SubPc) derivatives for photovoltaic applications. Opt Mater 107:110154

53. Sikandar R et al (2021) Tuning the optoelectronic properties of oligothienyl silane derivatives and their photovoltaic properties. J Mol Graph Model 106:107918

54. Ans M et al (2020) Designing alkoxy-induced based high performance near infrared sensitive small molecule acceptors for organic solar cells. J Mol Liq 305:112829

55. Köse ME (2012) Evaluation of acceptor strength in thiophene coupled donor–acceptor chromophores for optimal design of organic photovoltaic materials. J Phys Chem A 116(51):12503–12509

56. Ans M et al (2019) Designing dithienothiophene (DTT)-based donor materials with efficient photovoltaic parameters for organic solar cells. J Mol Model 25(8):1–12

57. Lee J et al (2018) Bandgap narrowing in non-fullerene acceptors: single atom substitution leads to high optoelectronic response beyond 1000 nm. Adv Energy Mater 8(24):1801212

58. Ans M et al (2022) Simultaneously enhanced efficiency of eco-friendly structural characterization of the dithienocyclopentacarbazole donor based acceptors with narrow bandgap for high-performance organic solar cells. J Phys D Appl Phys 55(23):235501

59. Ans M et al (2019) Designing of non-fullerene 3D star-shaped acceptors for organic solar cells. J Mol Model 25(5):1–12

60. Ans M et al (2019) Opto-electronic properties of non-fullerene fused-undecacyclic electron acceptors for organic solar cells. Comput Mater Sci 159:150–159

61. Ahmed S, Kalita DJ (2020) End-capped group manipulation of non-fullerene acceptors for efficient organic photovoltaic solar cells: a DFT study. Phys Chem Chem Phys 22(41):23586–23596

62. Hachi M et al (2020) New small organic molecules based on thieno [2, 3-b] indole for efficient bulk heterojunction organic solar cells: a computational study. Mol Phys 118(8):e1662956

63. Ans M et al (2019) Development of fullerene free acceptors molecules for organic solar cells: a step way forward toward efficient organic solar cells. Comput Theor Chem 1161:26–38

64. Ans M et al (2019) Designing indacenodithiophene based non-fullerene acceptors with a donor–acceptor combined bridge for organic solar cells. RSC Adv 9(7):3605–3617

65. Dennler G et al (2008) Design rules for donors in bulk-heterojunction tandem solar cells towards 15% energy-conversion efficiency. Adv Mater 20(3):579–583

66. Khan MI et al (2022) End-capped group modification on cyclopentadithiophene based non-fullerene small molecule acceptors for efficient organic solar cells; a DFT approach. J Mol Graph Model 113:108162

67. Yaqoob U et al (2021) Structural, optical and photovoltaic properties of unfused Non-Fullerene acceptors for efficient solution processable organic solar cell (Estimated PCE greater than 12.4%): A DFT approach. J Mol Liq 341:117428

68. Green MA (1981) Solar cell fill factors: general graph and empirical expressions. Solid State Electron 24(8):788–789